

Fullerene Rotational Dynamics Generate Disordered Configurations That Suppress Thermal Conductivity in Superatomic Crystals

Qi Liang,^{‡a,b} Matthew Bartnof,^{‡b} Ya-Ling He,^a Jonathan A. Malen,^b and Alan J. H. McGaughey^{*b}

^a *Key Laboratory of Thermo-Fluid Science and Engineering of Ministry of Education, School of Energy and Power Engineering, Xi'an Jiaotong University, Xi'an, Shaanxi, 710049, China.*

^b *Department of Mechanical Engineering, Carnegie Mellon University, Pittsburgh, Pennsylvania 15213, USA. E-mail: mcgaughey@cmu.edu*

[‡] These authors contributed equally to this work.

Contents

S1 Atomic Structure	2
S2 Bulk Modulus	12
S3 Thermal Conductivity	14
S4 Carbon Atom Trajectories	16
S5 C ₆₀ Relative Angle Distribution	18
S6 Rotational Potential Energy Barrier	20

S1 Atomic Structure

We downloaded the ‘mol2’ files for the superatomic crystals (SACs) from the CCDC¹ to build the structures for the MD simulations. All structures were initially built with the experimental unit cell parameters (i.e., lattice constants and angles) and then relaxed in the *NPT* ensemble (i.e., constant number of atoms N , pressure P , and temperature T) to get the zero-pressure unit cell parameters. The methodology for $[\text{C}_{60}]$ and the binary SACs $[\text{Co}_6\text{Se}_8(\text{PEt}_3)_6][\text{C}_{60}]_2$ ($[\text{CoSe}][\text{C}_{60}]_2$) and $[\text{Co}_6\text{Te}_8(\text{PEt}_3)_6][\text{C}_{60}]_2$ ($[\text{CoTe}][\text{C}_{60}]_2$) is described in the main text.

We also studied the unary SACs $[\text{Co}_6\text{S}_8(\text{PEt}_3)_6][\text{C}_7\text{H}_8]$ ($[\text{CoS}]$), $[\text{Co}_6\text{Se}_8(\text{PEt}_3)_6][\text{C}_7\text{H}_8]$ ($[\text{CoSe}]$) and $[\text{Co}_6\text{Te}_8(\text{PEt}_3)_6]$ ($[\text{CoTe}]$). At the experimental temperatures where data are available, the space group of $[\text{CoS}]$ is $\text{R}\bar{3}$ (100 K and 293 K) and the space group of $[\text{CoTe}]$ is $\text{P}\bar{1}$ (100 K). $[\text{CoSe}]$ experiences a phase transition from $\text{P}\bar{1}$ to $\text{R}\bar{3}$ between temperatures of 100 K and 293 K. $[\text{CoS}]$ and $[\text{CoSe}]$ contain one toluene molecule per cluster, which freely rotates within the space between the superatoms. For the unary SACs with space group $\text{R}\bar{3}$, the three side lengths of the simulation box were controlled independently, while the angles were fixed at the experimental values. For $[\text{CoSe}]$ with space group $\text{P}\bar{1}$, the three side lengths and the three angles of the simulation box were controlled independently. For $[\text{CoTe}]$, the three side lengths and the three angles of the simulation box were controlled independently at a temperature of 100 K. The angles were then fixed at the values calculated at a temperature of 100 K when running the *NPT* ensemble simulations to determine the higher temperature lattice constants.

The crystal structures and obtained zero-pressure unit cell parameters for all studied SACs are provided in Figures S1-S9 and Tables S1-S9. Experimental data are included for comparison.^{2,3}

Input and potential generating files for our implementation of the UFF for SACs in LAMMPS is available as part of the Supplementary Information. See “SAC_UFF.lt” for all the Universal Force Field parameters as calculated by OpenBabel⁴ in a format compatible with MolTemplate.⁵ See the data files for the atomic positions at a temperature of 300 K, using the base files O’Brien et al. submitted to the CCDC¹ with atomic charges calculated using the extended charge equilibration method⁶ as calculated by OpenBabel⁴.

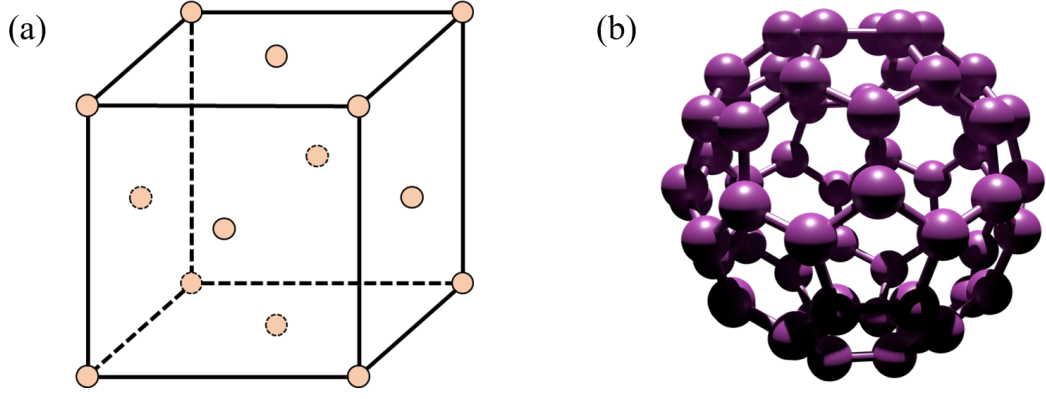


Figure S1: (a) Crystal structure and (b) basis of $[C_{60}]$ ($Fm\bar{3}m$). C = purple.

Table S1: Lattice constant of $[C_{60}]$ ($Fm\bar{3}m$). $\alpha = \beta = \gamma = 90^\circ$.

T (K)	Experimental data		Predicted data	
	$a/b/c$ (\AA)	Density (g/cm^3)	$a/b/c$ (\AA)	Density (g/cm^3)
25	14.0348	1.7300	13.8311	1.8093
50	14.0430	1.7269	13.8358	1.8074
75	14.0512	1.7239	13.8412	1.8051
100	14.0594	1.7209	13.8462	1.8027
125	14.0676	1.7179	13.8523	1.8004
150	14.0758	1.7149	13.8578	1.7986
175	14.0840	1.7119	13.8643	1.7960
200	14.0922	1.7089	13.8742	1.7930
225	14.1004	1.7059	13.9008	1.7824
250	14.1086	1.7030	13.9069	1.7799
275	14.1168	1.7000	13.9128	1.7774
300	14.1250	1.6970	13.9188	1.7742

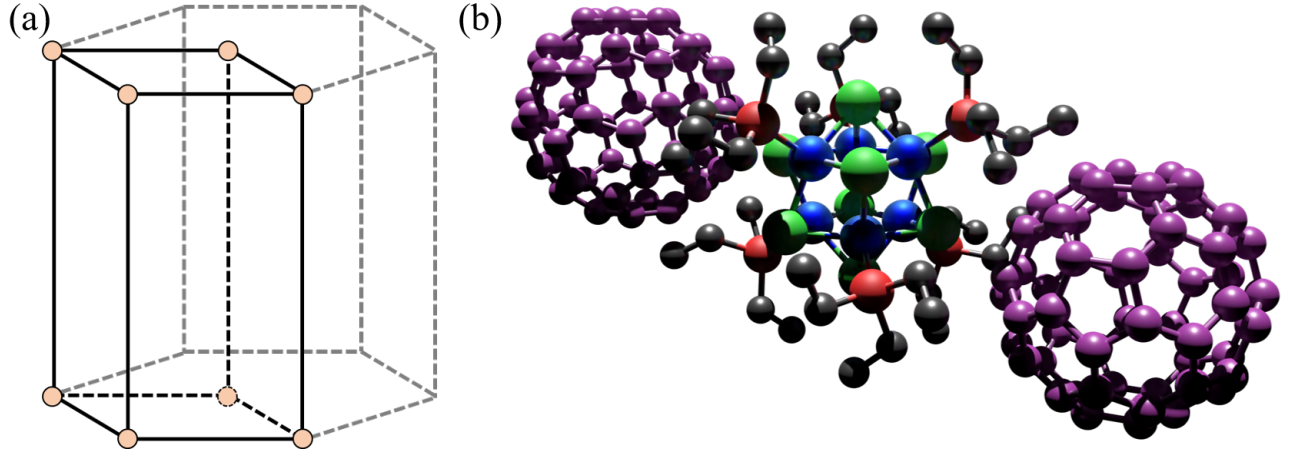


Figure S2: (a) Crystal structure and (b) basis of $[\text{CoSe}][\text{C}_{60}]_2$ ($P\bar{3}$). Co = blue, Se = green, P = red, C in CoSe = black, C in C_{60} = purple. Hydrogen atoms are removed to clarify the view.

Table S2: Lattice constants of $[\text{CoSe}][\text{C}_{60}]_2$ ($P\bar{3}$). $\alpha = \beta = 90^\circ, \gamma = 120^\circ$.

T (K)	Experimental data			Predicted data		
	a/b (Å)	c (Å)	Density (g/cm ³)	a/b (Å)	c (Å)	Density (g/cm ³)
25				15.9284	12.2766	1.9303
50				15.9281	12.3033	1.9260
75				15.9275	12.3264	1.9227
100	15.7282	12.5180	1.9415	15.8814	12.4316	1.9178
125	15.7619	12.5214	1.9327	15.8809	12.4518	1.9148
150	15.7562	12.5521	1.9294	15.8931	12.4713	1.9088
175	15.7555	12.5483	1.9301	15.8915	12.4929	1.9051
200	15.8376	12.4483	1.9255	15.8984	12.5173	1.8999
250	15.8702	12.4871	1.9117	15.9069	12.5603	1.8911
300	15.8893	12.5167	1.9026	15.9171	12.5981	1.8843

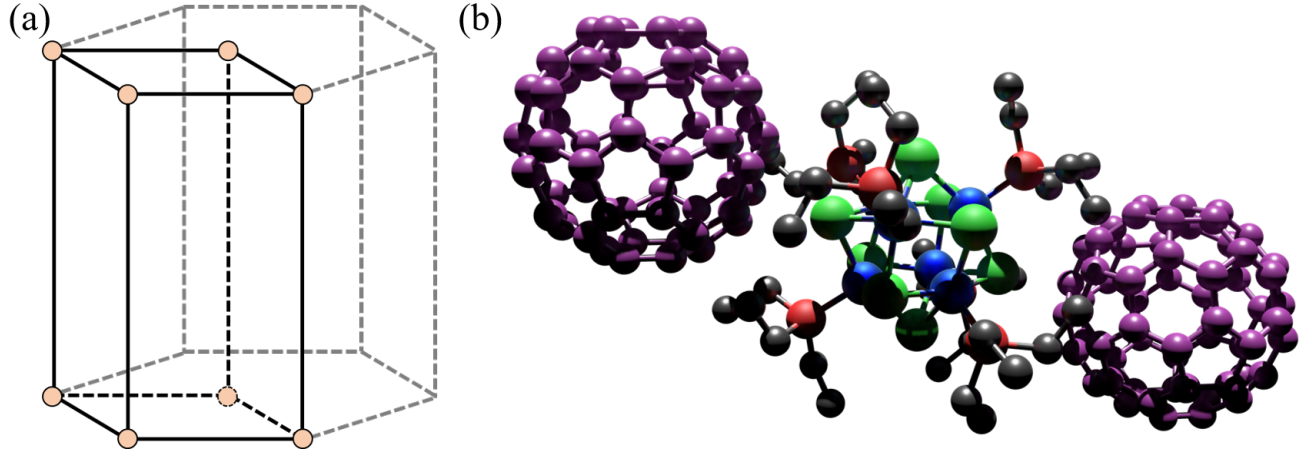


Figure S3: (a) Crystal structure and (b) basis of $[\text{CoSe}][\text{C}_{60}]_2$ ($\text{P}\bar{3}\text{m}1$). Co = blue, Se = green, P = red, C in CoSe = black, C in C_{60} = purple. Hydrogen atoms are removed to clarify the view.

Table S3: Lattice constants of $[\text{CoSe}][\text{C}_{60}]_2$ ($\text{P}\bar{3}\text{m}1$). $\alpha = \beta = 90^\circ, \gamma = 120^\circ$.

T (K)	Experimental data			Predicted data		
	a/b (Å)	c (Å)	Density (g/cm ³)	a/b (Å)	c (Å)	Density (g/cm ³)
25				15.9933	12.3432	1.9041
50				15.9836	12.3782	1.9015
100	15.7282	12.5180	1.9415	16.0131	12.3684	1.8958
150	15.7562	12.5521	1.9294	16.0217	12.4165	1.8855
200	15.8376	12.4483	1.9255	16.0344	12.4541	1.8774
250	15.8702	12.4871	1.9117	16.0406	12.5052	1.8703
300	15.8893	12.5167	1.9026	16.0499	12.5493	1.8581

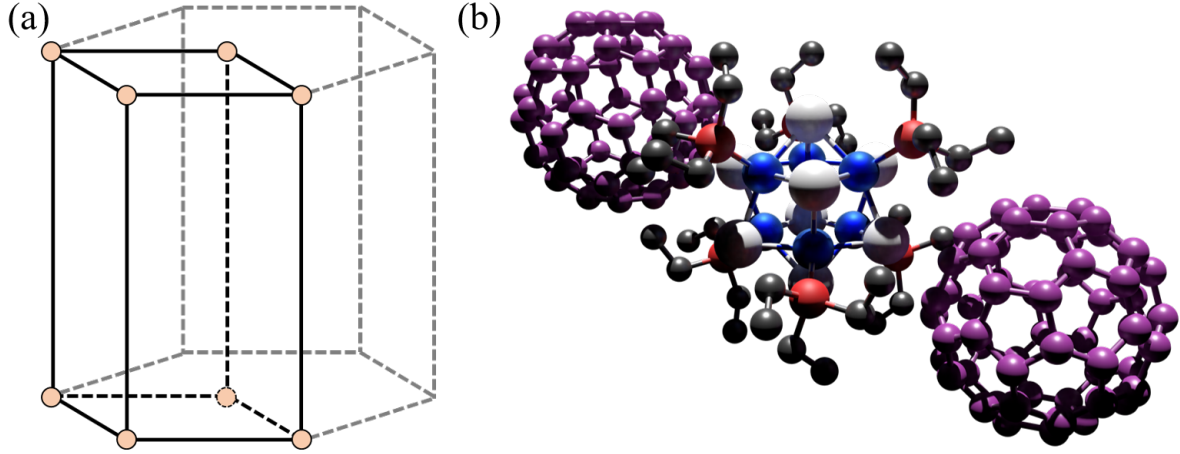


Figure S4: (a) Crystal structure and (b) basis of $[\text{CoTe}][\text{C}_{60}]_2$ ($P\bar{3}$). Co = blue, Te = white, P = red, C in CoTe = black, C in C_{60} = purple. Hydrogen atoms are removed to clarify the view.

Table S4: Lattice constants of $[\text{CoTe}][\text{C}_{60}]_2$ ($P\bar{3}$). $\alpha = \beta = 90^\circ, \gamma = 120^\circ$.

T (K)	Experimental data			Predicted data		
	a/b (Å)	c (Å)	Density (g/cm ³)	a/b (Å)	c (Å)	Density (g/cm ³)
25				16.1784	12.3185	2.0958
50				16.1793	12.3445	2.0921
75				16.1944	12.3382	2.0888
100	16.0555	12.2192	2.1456	16.2003	12.3476	2.0854
125	16.0559	12.2604	2.1382	16.1964	12.3925	2.0788
150	16.0473	12.3338	2.1278	16.1947	12.4348	2.0719
175	16.0428	12.3957	2.1184	16.1974	12.4627	2.0680
200	15.9955	12.4066	2.1290	16.1997	12.4922	2.0623
250	16.0702	12.4759	2.0970	16.2073	12.5395	2.0520
300	16.0906	12.5353	2.0820	16.2178	12.5782	2.0426

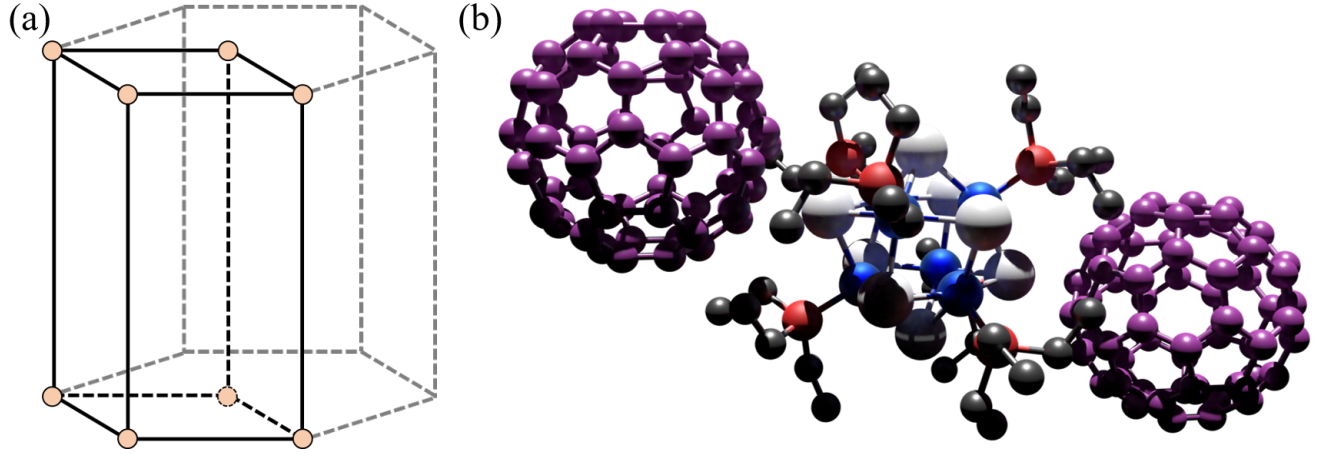


Figure S5: (a) Crystal structure and (b) basis of $[\text{CoTe}][\text{C}_{60}]_2$ ($\text{P}\bar{3}\text{m}1$). Co = blue, Te = white, P = red, C in CoTe = black, C in C_{60} = purple. Hydrogen atoms are removed to clarify the view.

Table S5: Lattice constants of $[\text{CoTe}][\text{C}_{60}]_2$ ($\text{P}\bar{3}\text{m}1$). $\alpha = \beta = 90^\circ, \gamma = 120^\circ$.

T (K)	Experimental data			Predicted data		
	a/b (Å)	c (Å)	Density (g/cm ³)	a/b (Å)	c (Å)	Density (g/cm ³)
25				16.1500	12.3891	2.0915
50				16.1680	12.3880	2.0871
100	16.0555	12.2192	2.1456	16.1957	12.3607	2.0838
150	16.0473	12.3338	2.1278	16.1954	12.4322	2.0733
200	15.9955	12.4066	2.1290	16.1997	12.4912	2.0601
250	16.0702	12.4759	2.0970	16.2074	12.5396	2.0517
300	16.0906	12.5353	2.0820	16.2176	12.5792	2.0437

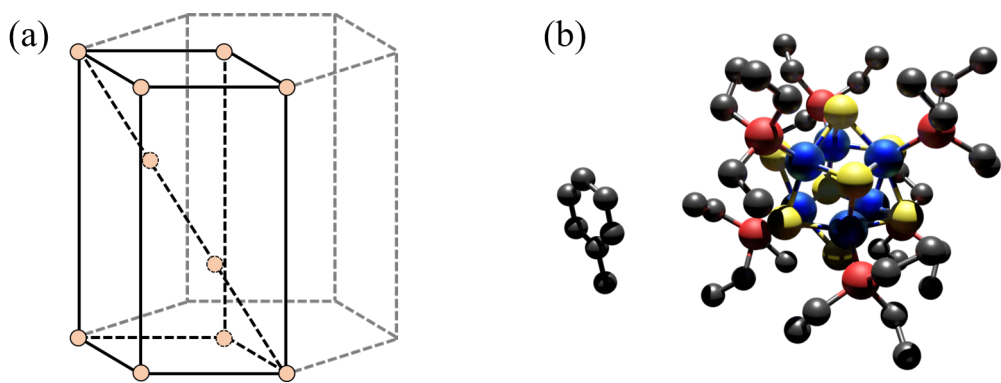


Figure S6: (a) Crystal structure and (b) basis of $[\text{CoS}] (\text{R}\bar{3})$. Co = blue, S = yellow, P = red, C = black. Hydrogen atoms are removed to clarify the view.

Table S6: Lattice constants of $[\text{CoS}] (\text{R}\bar{3})$. $\alpha = \beta = 90^\circ, \gamma = 120^\circ$.

T (K)	Experimental data			Predicted data		
	a/b (Å)	c (Å)	Density (g/cm ³)	a/b (Å)	c (Å)	Density (g/cm ³)
100	16.7652	19.2013	1.5058	17.3716	19.5400	1.3766
150				17.4133	19.5790	1.3673
200				17.4574	19.6106	1.3582
250				17.5018	19.6384	1.3495
293	16.9491	19.2886	1.4650			
300				17.5492	19.6691	1.3401

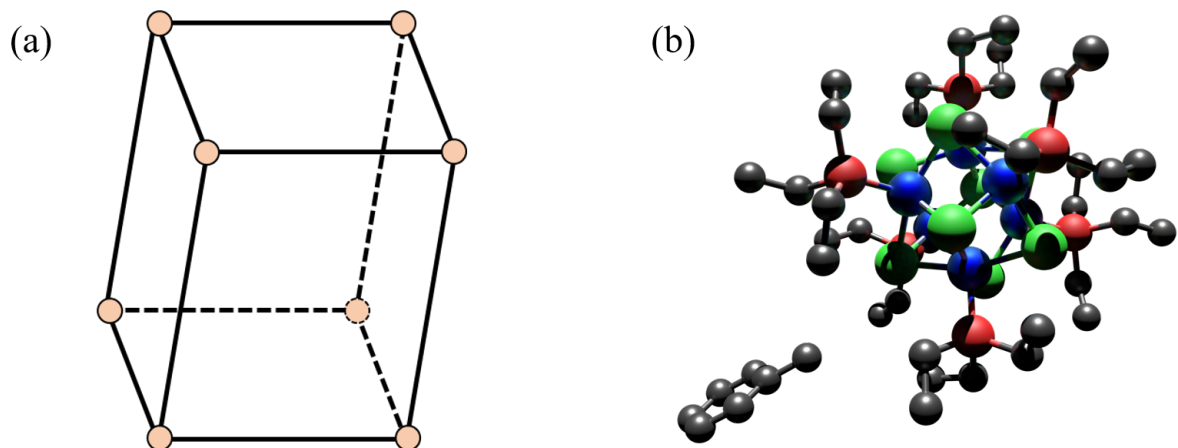


Figure S7: (a) Crystal structure and (b) basis of $[\text{CoSe}] (\text{P}\bar{1})$. Co = blue, Se = green, P = red, C = black. Hydrogen atoms are removed to clarify the view.

Table S7: Lattice constants and angles of $[\text{CoSe}] (\text{P}\bar{1})$. The measured lattice constants and angles at a temperature of 100 K are $a = 11.6534 \text{ \AA}$, $b = 11.7631 \text{ \AA}$, $c = 11.7664 \text{ \AA}$, $\alpha = 93.4394^\circ$, $\beta = 90.5354^\circ$, and $\gamma = 94.1205^\circ$, and the density is 1.8473 g/cm^3 .

T (K)	a (\AA)	b (\AA)	c (\AA)	α ($^\circ$)	β ($^\circ$)	γ ($^\circ$)	Density (g/cm^3)
100	11.8147	11.8918	12.1765	93.4430	89.9499	94.4722	1.7425
150	11.8502	11.9517	12.1989	93.4678	90.1323	94.4007	1.7253
200	11.8925	12.0075	12.2160	93.4313	90.3615	94.3146	1.7086
250	12.1135	12.1095	12.1164	92.8980	92.8204	92.8316	1.6755
300	12.1570	12.1516	12.1541	92.9584	92.9484	92.8839	1.6589

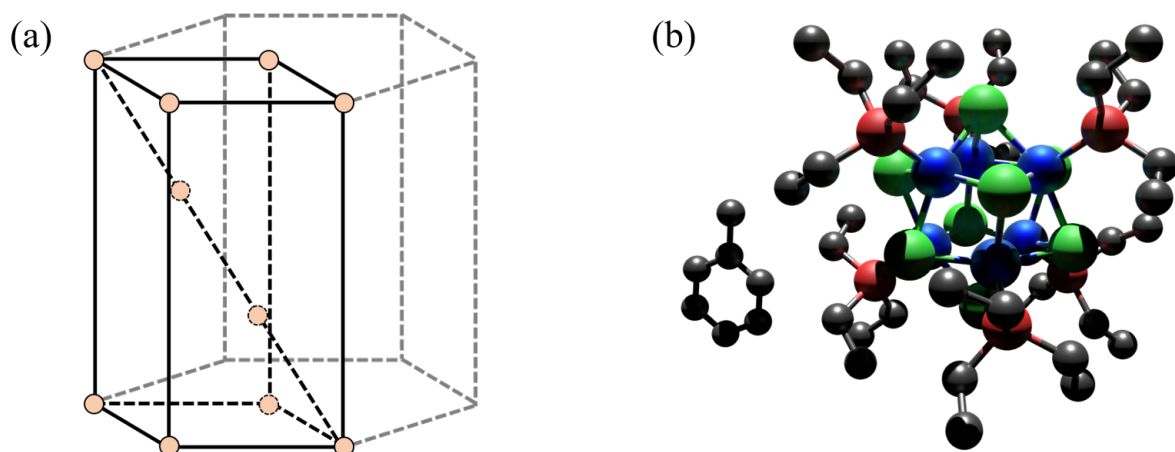


Figure S8: (a) Crystal structure and (b) basis of $[\text{CoSe}] (\text{R}\bar{3})$. Co = blue, Se = green, P = red, C = black. Hydrogen atoms are removed to clarify the view.

Table S8: Lattice constants of $[\text{CoSe}] (\text{R}\bar{3})$. $\alpha = \beta = 90^\circ, \gamma = 120^\circ$. The measured lattice constants at a temperature of 293 K are $a = b = 17.1316 \text{ \AA}$, and $c = 19.4810 \text{ \AA}$, and the density is 1.7972 g/cm^3 .

T (K)	a/b (\AA)	c (\AA)	Density (g/cm^3)
100	17.3104	19.8131	1.7309
150	17.3931	19.8683	1.7097
200	17.4931	19.9022	1.6873
250	17.5635	19.9251	1.6719
300	17.6259	19.9537	1.6577

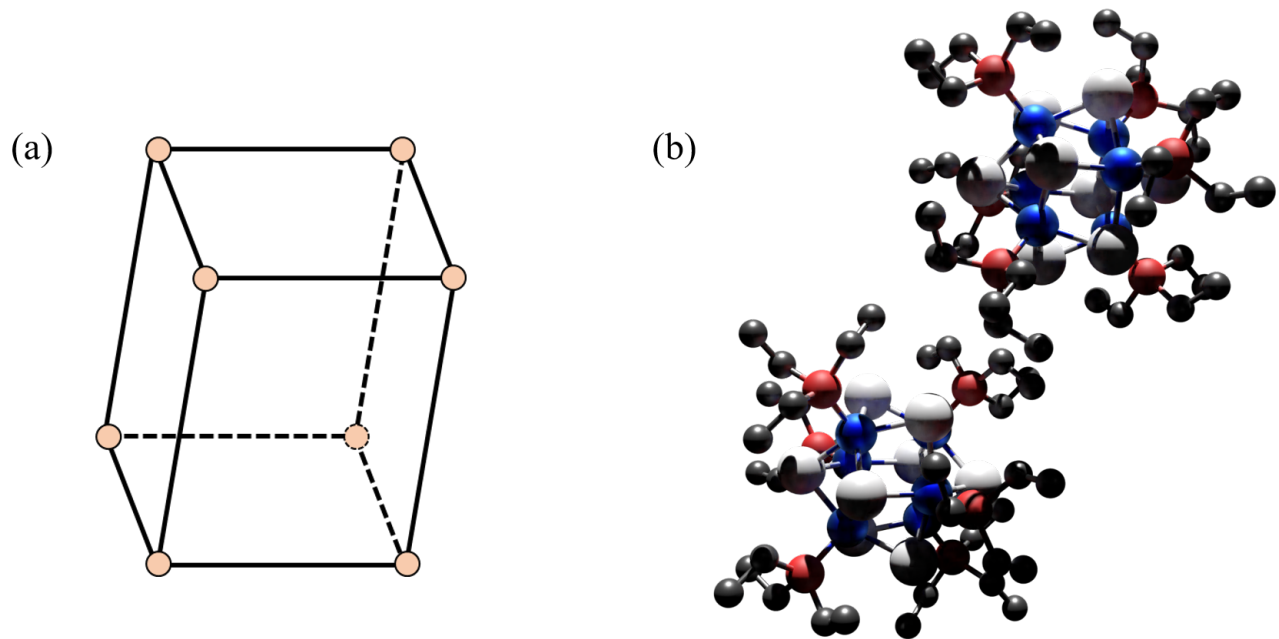


Figure S9: (a) Crystal structure and (b) basis of $[\text{CoTe}] (\text{P}\bar{1})$. Co = blue, Te = white, P = red, C = black. Hydrogen atoms are removed to clarify the view.

Table S9: Lattice constants of $[\text{CoTe}] (\text{P}\bar{1})$. $\alpha = 88.648^\circ, \beta = 86.025^\circ, \gamma = 72.757^\circ$. The measured lattice constants at a temperature of 100 K are $a = 12.1664 \text{ \AA}$, $b = 13.0458 \text{ \AA}$, and $c = 20.1918 \text{ \AA}$, and the density is 2.2918 g/cm^3 .

T (K)	a (\AA)	b (\AA)	c (\AA)	Density (g/cm^3)
100	12.5349	13.1153	20.4883	2.1561
150	12.5503	13.1309	20.5519	2.1442
200	12.5661	13.1463	20.6171	2.1322
250	12.5823	13.1627	20.6843	2.1199
300	12.5997	13.1793	20.7519	2.1074

S2 Bulk Modulus

The elements of the stiffness tensor C_{ij} are given by

$$C_{ij} = \frac{\sigma_i}{\epsilon_j}, \quad (\text{S1})$$

where σ_i is a component of the stress tensor and ϵ_j is a component of the strain tensor based on the Voigt notation where $i, j = 1, 2, \dots, 6$. In our simulations, ϵ_j is set to be 0.01. To get the stiffness tensor, we run an *NVT* simulation (i.e., constant number of atoms, volume, and temperature) using deformed simulation boxes with the strain ϵ_j for 2×10^6 time steps. Then, the stress tensor is collected every 10 time steps and obtained by averaging the last 10^6 time steps.

Once the stiffness tensor is obtained, the effective bulk modulus B_{VRH} can be estimated by the Voigt-Reuss-Hill averaging scheme from^{7,8}

$$B_{\text{VRH}} = \frac{B_V + B_R}{2}, \quad (\text{S2})$$

where B_V and B_R are the effective bulk moduli obtained by Voigt averaging and Reuss averaging. The Voigt averaging scheme is based on the stiffness tensor:

$$B_V = \frac{A + 2B}{3}, \quad (\text{S3})$$

where

$$A = \frac{C_{11} + C_{22} + C_{33}}{3}, \quad B = \frac{C_{23} + C_{13} + C_{12}}{3}. \quad (\text{S4})$$

The Reuss averaging scheme is based on the compliance tensor S_{ij} , the inverse of the stiffness tensor:

$$B_R = \frac{1}{3a + 6b}, \quad (\text{S5})$$

where

$$a = \frac{S_{11} + S_{22} + S_{33}}{3}, \quad b = \frac{S_{23} + S_{13} + S_{12}}{3}. \quad (\text{S6})$$

The calculated bulk moduli of the unary and binary SACs are plotted in Figure S10 as a function of temperature. [CoTe] is the stiffest unary SAC, while [CoS] and both phases of [CoSe] have similar values. For the binary SACs, [CoSe][C₆₀]₂ (P $\bar{3}$) is the stiffest, while [CoSe][C₆₀]₂ (P $\bar{3}$ m1) is the softest. The effects of phase is not as significant on the bulk modulus of [CoTe][C₆₀]₂ as compared to [CoSe][C₆₀]₂.

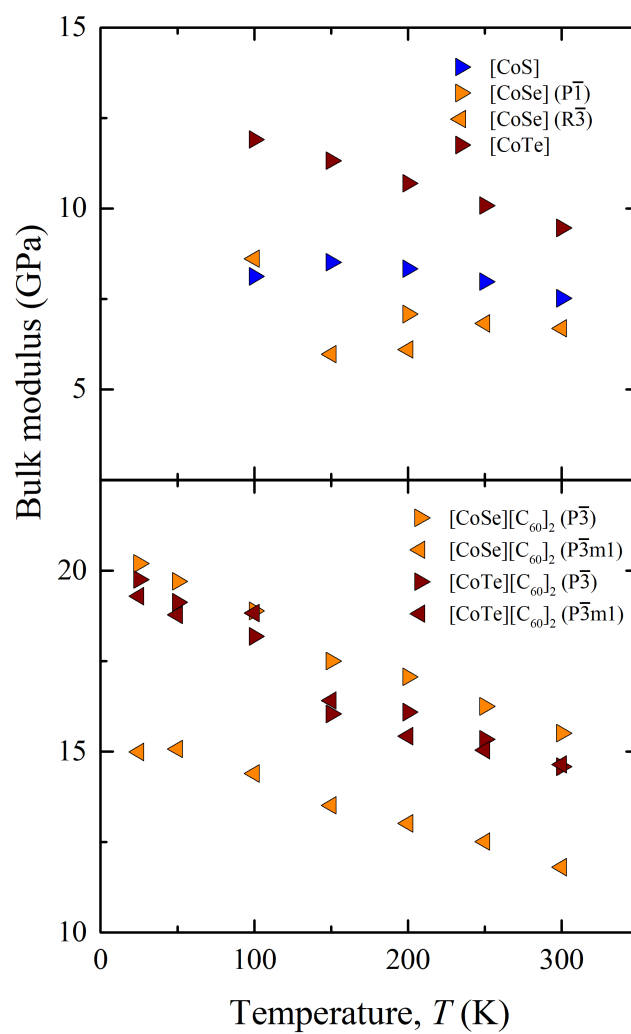


Figure S10: MD-predicted bulk moduli of the unary and binary SACs

S3 Thermal Conductivity

The thermal conductivity in the α direction, k_α , is predicted using the Green-Kubo method from

$$\kappa_\alpha = \frac{1}{k_B V T^2} \int_0^\infty \langle q_\alpha(t) q_\alpha(0) \rangle dt, \quad (\text{S7})$$

where q_α is the α -direction heat current, k_B is Boltzmann constant, V is the volume of the simulation box and T is temperature. $\langle q_\alpha(t) q_\alpha(0) \rangle$ is the heat current autocorrelation function (HCACF). The effect of the simulation box size on the predicted thermal conductivity at a temperature of 300 K for $[\text{C}_{60}]$ and $[\text{CoTe}][\text{C}_{60}]_2$ is presented in Table S10. The results suggest that a $3 \times 3 \times 3$ unit cell system is sufficient to obtain a sized-converged value of thermal conductivity.

Table S10: Size-dependent thermal conductivities of $[\text{C}_{60}]$ and $[\text{CoTe}][\text{C}_{60}]_2$ ($\text{P}\bar{3}\text{m1}$) at a temperature of 300 K.

Box size	$[\text{C}_{60}]$	$[\text{CoTe}][\text{C}_{60}]_2$ ($\text{P}\bar{3}\text{m1}$)	
(unit cells)	$a/b/c$ (W/m-K)	a/b (W/m-K)	c (W/m-K)
$2 \times 2 \times 2$	0.358 ± 0.025	0.157 ± 0.006	0.180 ± 0.004
$3 \times 3 \times 3$	0.390 ± 0.054	0.171 ± 0.004	0.210 ± 0.005
$4 \times 4 \times 4$	0.399 ± 0.018	0.183 ± 0.010	0.188 ± 0.002

The predicted thermal conductivities of the unary SACs are plotted in Figures S11(a)-S11(d) as a function of temperature. The calculation method for unary SACs is the same as that for binary SACs described in the main text. The predicted thermal conductivity magnitudes and trends agree moderately well with the experimental data³. All the unary SACs have an amorphous-like thermal conductivity, as observed in the experiments.

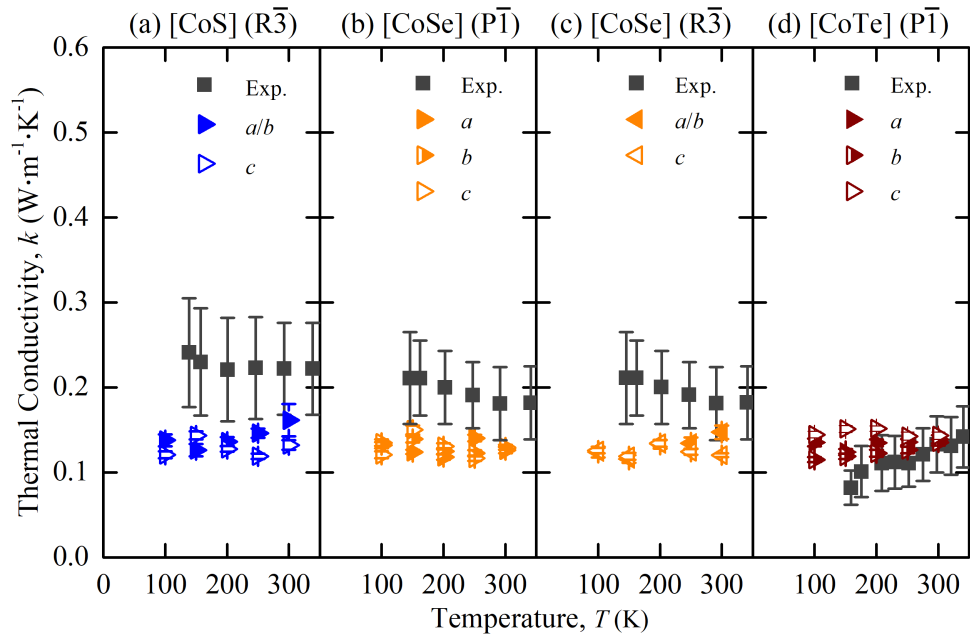


Figure S11: MD-predicted thermal conductivities of the unary SACs and experimental data.³ [CoSe] experiences a phase transition from $\text{P}\bar{1}$ to $\text{R}\bar{3}$ between temperatures of 100 K and 293 K. Because the phase transition temperature is unknown, we plot the [CoSe] experimental data in both (b) and (c).

S4 Carbon Atom Trajectories

Atomic trajectories for carbon atoms in the binary SACs are provided in Figures S12-S15 at various temperatures to supplement those given in the main text in Figures 4(a)-4(c). These plots clearly show the fullerene cages transitioning from librating to freely rotating with increasing temperature.

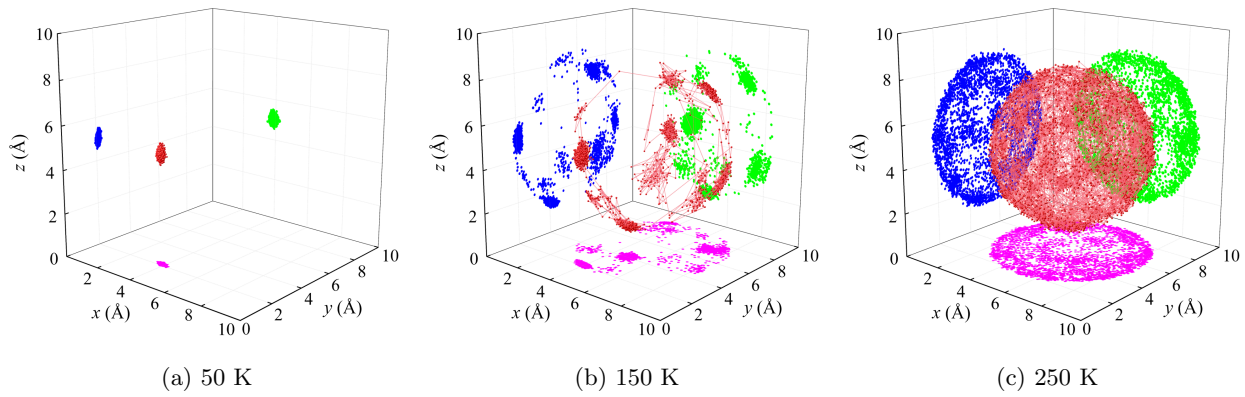


Figure S12: Trajectories of a carbon atom in $[\text{CoSe}][\text{C}_{60}]_2$ ($P\bar{3}$) at various temperatures.

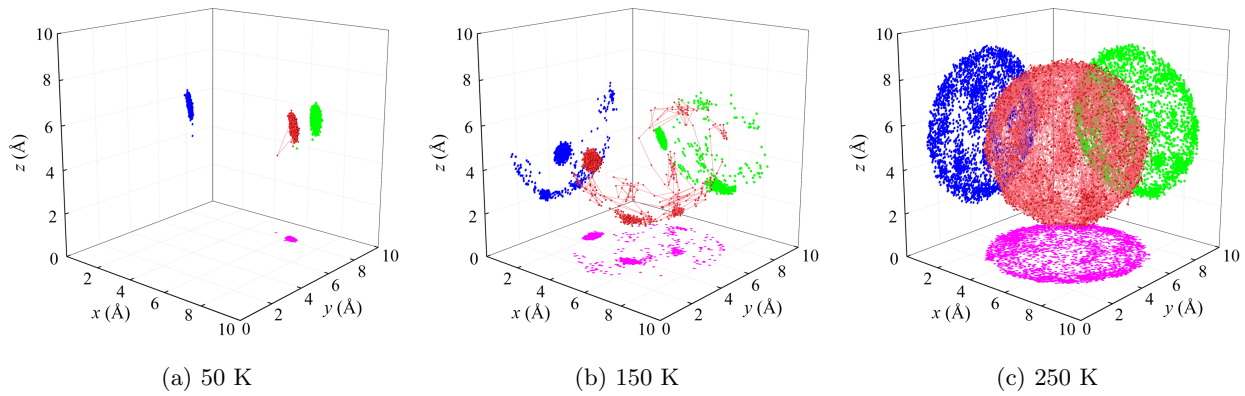


Figure S13: Trajectories of a carbon atom in $[\text{CoSe}][\text{C}_{60}]_2$ ($P\bar{3}m1$) at various temperatures.

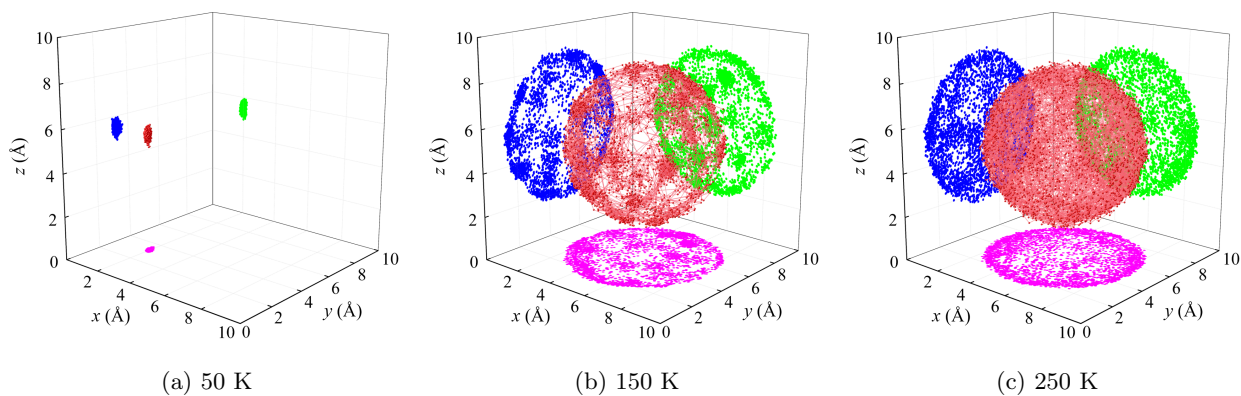


Figure S14: Trajectories of a carbon atom in $[\text{CoTe}][\text{C}_{60}]_2$ ($\text{P}\bar{3}$) at various temperatures.

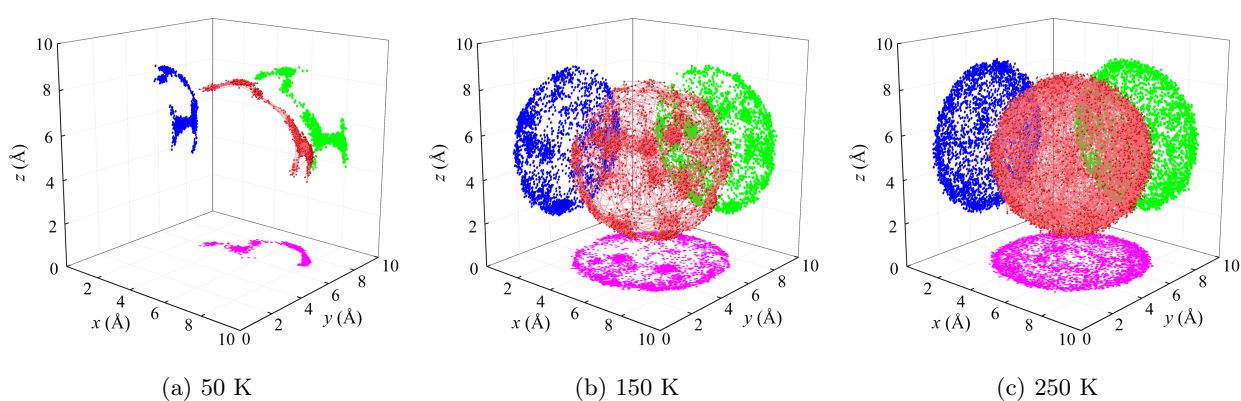


Figure S15: Trajectories of a carbon atom in $[\text{CoTe}][\text{C}_{60}]_2$ ($\text{P}\bar{3}\text{m}1$) at various temperatures.

S5 C₆₀ Relative Angle Distribution

The temperature-dependent distribution of the minimum relative angle θ between pairs of C₆₀ molecules are plotted in Figures S16 ([C₆₀]) and S17(a)-S17(d) (binary SACs). In [C₆₀], below a temperature of about 125 K, the relative angle between two molecules is less than 10° and there is orientational order. As the temperature increases, the distributions for both [C₆₀] and the binary SACs widen, indicating that the cages are exploring more of the rotational phase space while still coordinating to their neighboring molecules. Above 212.5 K for pure [C₆₀], the relative angle is nearly evenly distributed between 0 and 37.5°. The molecules are orientational disordered as there is no coordination of the angles of neighboring molecules. This phenomenon occurs for both binary compounds with the $P\bar{3}$ crystal structure. The $P\bar{3}m1$ crystal structures do not experience the narrowing of distribution at low temperatures because they are orientationally disordered at all temperatures.

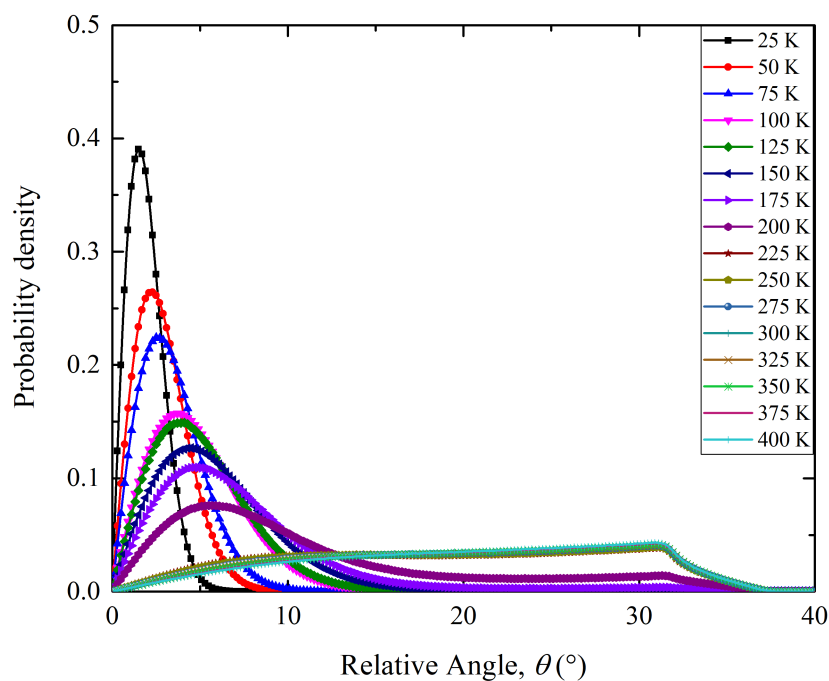


Figure S16: Distribution of the minimum relative angle between C₆₀ molecules in [C₆₀].

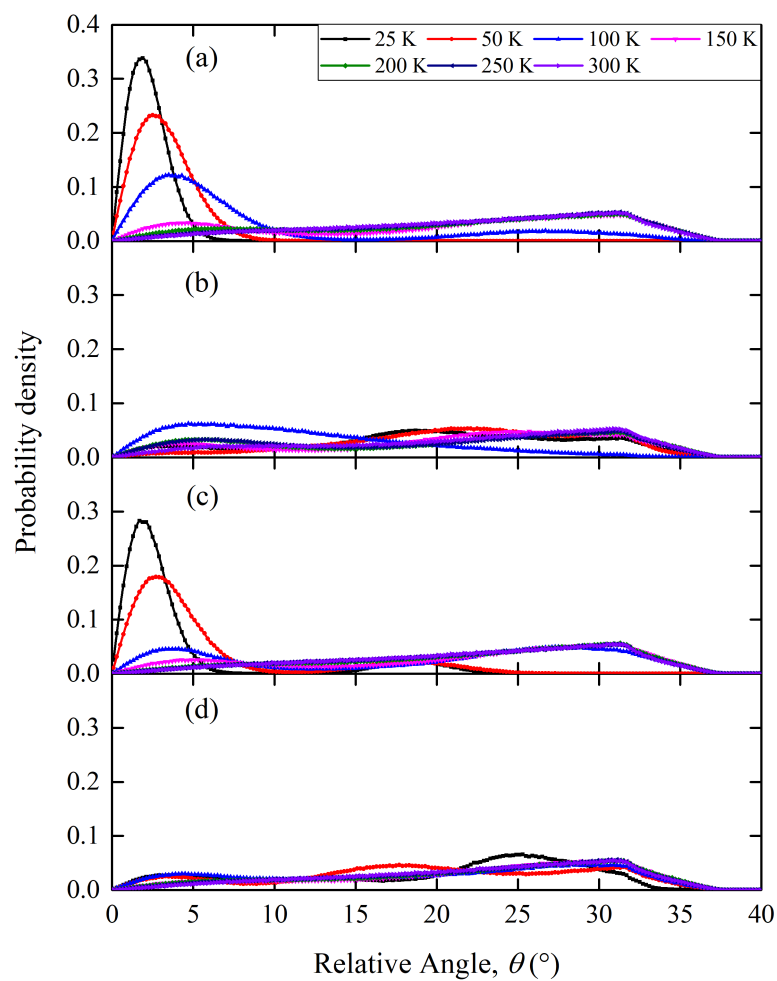


Figure S17: Distribution of the minimum relative angle between C_{60} molecules in (a) $[CoSe][C_{60}]_2$ ($P\bar{3}$), (b) $[CoSe][C_{60}]_2$ ($P\bar{3}m1$), (c) $[CoTe][C_{60}]_2$ ($P\bar{3}$), (d) $[CoTe][C_{60}]_2$ ($P\bar{3}m1$).

S6 Rotational Potential Energy Barrier

As shown in Table 1 of the main text, while there is negligible difference in the SA- C_{60} centroid-to-centroid distance for the various SACs, the C_{60} - C_{60} centroid distance does show variation. We built a toy model to calculate the rotational potential energy barrier between two C_{60} s as a function of their centroid-to-centroid spacing, as shown in Figure S18. We rotate the right C_{60} molecule and calculate the total system potential energy. The centroid-to-centroid distance is set as the value for a given SAC at a temperature of 300 K. The calculated potential energy landscape is plotted in Figure S19.

As the centroid-to-centroid distance increases, the energy barrier decreases rapidly. $[C_{60}]$ experiences the largest energy barrier of all the SACs studied. Among the binary SACs, $[CoSe][C_{60}]_2$ in the $P\bar{3}$ crystal structure has the highest energy barrier, followed by that of $[CoTe][C_{60}]_2$ in the $P\bar{3}$ crystal structure. The energy barrier for the two $P\bar{3}m1$ phases is essentially zero, which is what leads them to be orientationally disordered at all temperatures and to exhibit an amorphous-like thermal conductivity. The thermal conductivities of $[C_{60}]$ and the binary SACs exhibit a crystal-like behavior only when the energy barrier is high enough that the C_{60} s are orientationally ordered.

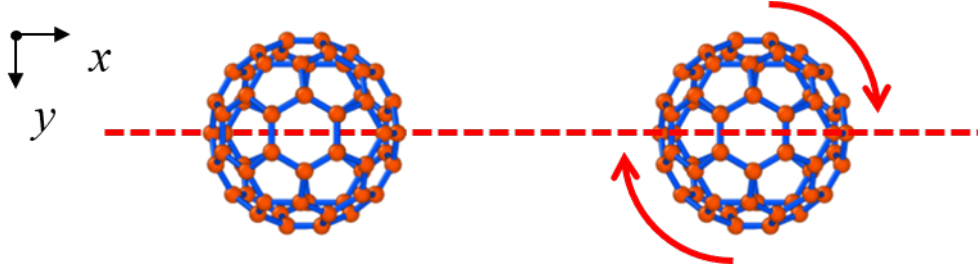


Figure S18: Model for calculating the rotational potential energy landscape and barrier.

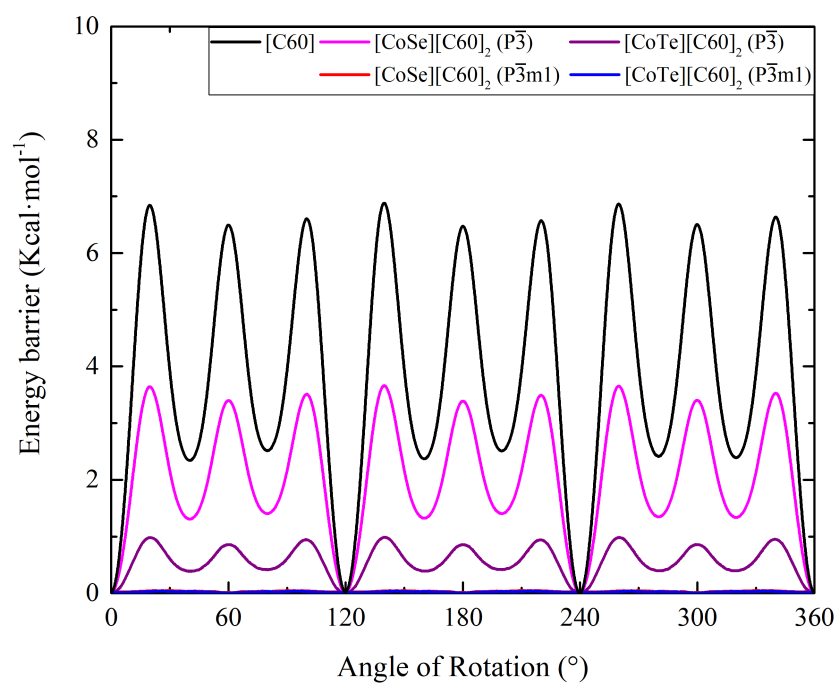


Figure S19: Potential energy landscape and barrier for rotating C_{60} molecules based on their separation as found in the SACs at a temperature of 300 K. The separation is 9.8420 Å for $[C_{60}]$, 9.9495 Å for $[CoSe][C_{60}]_2$ ($P\bar{3}$), 11.2408 Å for $[CoSe][C_{60}]_2$ ($P\bar{3}m1$), 10.1835 Å for $[CoTe][C_{60}]_2$ ($P\bar{3}$), and 11.3267 Å for $[CoTe][C_{60}]_2$ ($P\bar{3}m1$).

References

- [1] C. R. Groom, I. J. Bruno, M. P. Lightfoot and S. C. Ward, *Acta Crystallogr. B*, 2016, **72**, 171–179.
- [2] W. I. F. David, R. M. Ibberson and T. Matsuo, *Proceedings of the Royal Society of London. Series A: Mathematical and Physical Sciences*, 1993, **442**, 129–146.
- [3] W.-L. Ong, E. S. O’Brien, P. S. M. Dougherty, D. Paley, C. F. Higgs, A. J. H. McGaughey, J. A. Malen and X. Roy, *Nat. Mater.*, 2017, **16**, 83–88.
- [4] N. M. O’Boyle, M. Banck, C. A. James, C. Morley, T. Vandermeersch and G. R. Hutchison, *J. Cheminformatics*, 2011, **3**, 33.
- [5] A. Jewett, *Moltemplate*, <https://moltemplate.org>.
- [6] C. E. Wilmer, K. C. Kim and R. Q. Snurr, *J. Phys. Chem. Lett.*, 2012, **3**, 2506–2511.
- [7] A. Marmier, Z. A. Lethbridge, R. I. Walton, C. W. Smith, S. C. Parker and K. E. Evans, *Comput. Phys. Commun*, 2010, **181**, 2102–115.
- [8] R. Gaillac, P. Pullumbi and F.-X. Coudert, *J. Phys. Condens. Matter*, 2016, **28**, 275201.